Journal of Power Sources 272 (2014) 845–859

Contents lists available at ScienceDirect

Journal of Power Sources

journal homepage: www.elsevier.com/locate/jpowsour

Carbon monoxide tolerant platinum electrocatalysts on niobium doped titania and carbon nanotube composite supports

William A. Rigdon*, Xinyu Huang

University of South Carolina, Mechanical Engineering Department, College of Engineering and Computing, 541 Main Street, Columbia, SC 29208, USA

HIGHLIGHTS

- Material characterization reveals structure and property of electrocatalysts on differing supports.
- Carbon composite supports with doped titania can improve CO tolerance of platinum catalysts.
- Hydrogen pumps are used to effectively qualify electrocatalyst behaviors in the anode of MEAs.
- Niobium doped titania supports showed resilient performance in hydrogen pump tests with CO.

ARTICLE INFO

Article history:
Received 18 June 2014
Received in revised form
2 September 2014
Accepted 4 September 2014
Available online 16 September 2014

Keywords:
CO tolerance
Catalyst support
Bifunctional mechanism
Hydrogen pump
Strong metal-support interaction
Schottky junction

ABSTRACT

In the anode of electrochemical cells operating at low temperature, the hydrogen oxidation reaction is susceptible to poisoning from carbon monoxide (CO) which strongly adsorbs on platinum (Pt) catalysts and increases activation overpotential. Adsorbed CO is removed by oxidative processes such as electrochemical stripping, though cleaning can also cause corrosion. One approach to improve the tolerance of Pt is through alloying with less-noble metals, but the durability of alloyed electrocatalysts is a critical concern. Without sacrificing stability, tolerance can be improved by careful design of the support composition using metal oxides. The bifunctional mechanism is promoted at junctions of the catalyst and metal oxides used in the support. Stable metal oxides can also form strong interactions with catalysts, as is the case for platinum on titania (TiO_x). In this study, niobium (Nb) serves as an electron donor dopant in titania. The transition metal oxides are joined to functionalized multi-wall carbon nanotube (CNT) supports in order to synthesize composite supports. Pt is then deposited to form electrocatalysts which are characterized before fabrication into anodes for tests as an electrochemical hydrogen pump. Comparisons are made between the control from Pt-CNT to Pt-TiO_x-CNT and Pt-$Ti_{0.9}Nb_{0.1}O_x$-CNT in order to demonstrate advantages.

1. Introduction

Electrocatalysts are an essential part of many electrochemical cells which are often assembled in challenging ways to design the most effective electrodes. Unfortunately, catalysts such as platinum (Pt) are expensive and often contribute substantially to the overall system cost. To reduce the amount needed, nanostructured Pt particles can be supported on conductive substrates that are intricately distributed into electrodes used for polymer electrolyte cells. In the anode of a fuel cell, the overpotential for oxidation of hydrogen (H_2) is relatively low when compared to the oxygen reduction reaction (ORR) of the cathode. However, presence of carbon monoxide (CO) in the hydrogen oxidation reaction (HOR) has a significant poisoning effect under typical operating conditions when active Pt sites become covered during exposure. At operation temperatures <100 °C, even low concentrations $\gtrsim$10 ppm CO can severely impact cell performance in a short time [1–3]. Electrode poisoning from CO in the fuel is one of the major challenges plaguing development of this technology. Therefore, a more resilient electrocatalyst in operations with CO can have very significant cost savings and deserves our attention [4].

Electrocatalyst properties of metals can depend on crystalline epitaxy, lattice strain, metal-ligand effects, and from their interfaces with adjoining compounds that could be a constituent phase of the support [5,6]. Although it is possible to alter the adsorption properties of CO on electrocatalysts by changing these parameters, the bifunctional mechanism has been well established for its removal once poisoned [7,8]. In the case of adsorbed CO on

* Corresponding author. Tel.: +1 (803) 777 1861; fax: +1 803 777 0137.
E-mail addresses: rigdonwa@email.sc.edu, warigdon@gmail.com (W.A. Rigdon).

http://dx.doi.org/10.1016/j.jpowsour.2014.09.054
0378-7753/

the catalyst, most is converted to carbon dioxide (CO_2). This effect is promoted when dually adsorbed species are involved in its oxidation as shown by Langmuir–Hinshelwood type reaction of Equation (1). Metal oxide (MO_x) phases formed in proximity to catalysts can serve this purpose by analogous ways to alloys with Pt [5,9]. Construction of a catalyst support with these materials could aid this property in addition to making it more durable.

$$MO_x - OH + Pt - CO_{ad} \rightarrow CO_2 + Pt + MO_x + H^+ + e^- \quad (1)$$

Improving tolerance to CO has been extensively investigated through alloying Pt with less-noble elements to promote bifunctional effects, although alloys can be limited by their stability. Advances with Pt alloys containing promoters such as Ru, Sn, and Mo are considered a state-of-the-art for CO tolerance, but these metals can also become compromised during operations [10–15]. From the perspective of stability, it is probably more rational to prepare those metals initially in a preferred oxidation state that form junctions with Pt [16–18]. In any case, contamination from the fuel adsorbs on anode catalysts; to restore their activity, oxygen pressure, temperature, and/or cell potential are generally increased to accomplish removal [19–21]. However, these processes can result in irreversible oxidation of the electrocatalyst as well. Unintended fuel starvation and cell reversal can also lead to high potentials, low pH, and conditions that cause degradation of this electrode [11,22,23]. These events all result in the loss of performance from electrocatalysts which can be corroded similarly to catalysts in the cathode of the fuel cell [24]. Electrocatalyst losses may be measured by changes in reversible features from cyclic voltammetry which correlate with active sites [25]. In alloys with Pt, the more active metal tends to be sacrificed while passivation occurs on the surface and noble metal lattice strain gets relieved [14,26]. Catalyst activity is lost, but secondary symptoms originating from this issue may also persist. For example, dissolved cations from alloyed metals can diffuse through proton channels and plate out in the electrolyte or other undesirable places [11,13]. Electrocatalyst degradation has a cumulative effect on performance which can eventually kill the cell; this paradox poses a challenge to the purpose of same materials which also make them work so well [27]. In the anode, tolerance to CO contamination should come without a big cost to stability for ideal electrocatalysts.

Electrocatalysts must be validated in electrodes with conditions similar to those found in real applications. Half-cells and rotating disk electrode (RDE) studies are essential in understanding fundamental behaviors to guide specific design, but results from full cell hardware are necessary in confirming the effectiveness of working electrodes. However, fuel cell testing complicates understanding of anode behavior due to sluggish ORR and other cathode effects. Electrochemical hydrogen pumps can provide more accurate characterization of the anode oxidation reactions. Protons formed in the anode are simply pumped across the membrane electrode assembly (MEA) and reduced at the cathode by applying potential. For the reference electrode, Pt black electrocatalysts dually serve as a cathode in the fast hydrogen evolution reaction. More sophisticated designs of this type can also efficiently serve an important role to purify diluted process flows and pressurize clean H_2 gas which is ideal for fuel cells. Application of potential provides for characterization of catalysts by a cyclic voltammetry technique which can be performed similarly to the hydrogen pump, except fuel has been purged from working electrodes by inert gas. From a diagnostic perspective, losses in pump performance and overpotentials can be relatively easy to quantify.

Transition metal oxides selected for this study were carefully chosen for stability and their interaction with Pt catalysts. The abundant element titanium (Ti) was picked as the major constituent with a minor addition of niobium (Nb) included as an electron donor in the oxide matrix. Both oxides have a wide passivation region overlapping the operating ranges used in the environment of related electrochemical cells, based on equilibrium Pourbaix (E_h-pH) diagrams [28,29]. It is imperative that materials used in catalysts should at least be prepared near to their equilibrium state (e.g. TiO_2 or Nb_2O_5) or else their surfaces will eventually adopt it during operations, resulting in irreversible transformations. The metal oxides are intended to serve several functional roles in the support. Titania can provide a stronger interaction with catalysts than carbon, improving durability by limiting diffusional growth [30–33]. The noble catalyst can also reduce the support metal oxidation state to form oxygen vacancies near the surface which facilitate the formation of hydroxyl (–OH) groups from the dissociation of water [34–38]. Titanium dioxide has been used for numerous catalytic applications and the science of its surface chemistry has been the single most investigated among transition metal systems [39,40]. In electrocatalysis, high conductivity is a necessary requirement and inadequate conduction of metal oxides has limited their use as support in related applications at low temperature. Although, an extensive number of recent reports have emerged which indicate there can be a synergistic combination for benefits to activity and stability from metal oxide supported electrocatalysts. Solely using metal oxide phases alone for the support is perhaps not practical because long range order of larger doped crystals (e.g. rutile) is typically needed to effectively form conductive electronic pathways, but the use of large crystals comes with a cost to available surface area [41–43]. Nevertheless, using metal oxides in conjunction with carbon could still be an effective approach to maintain suitable conductivity in the electrode without requiring a high catalyst loading [44–57]. Therefore, it is a goal to translate these conceivable developments into results that can be established in electrodes of low temperature cells.

The choice of doped metal oxides for this research is based on defect engineering principles that should be favored in the environment of the electrode. Defects are formed in host crystals by including irregular placement of elements that add charge carriers, often found in the gap state of oxides. Titanium (IV) dioxide has a wide band gap, but can be reduced by extra electrons formed during loss of oxygen atoms in the compound and it is typically referred to as n-type semiconductor. Adding defects contributes to both electron acceptor and donor properties, but often one type dominates. The selection of Nb as a donor dopant for Ti is based on its ionic radii, coordination number, and preferred valence state in the environment. Donor doping is ideal in reducing environments based on laws of mass action as suggested by the relationship of Equation (2) in Kröger–Vink notation [58,59]. At low oxygen concentrations found in the anode, oxygen vacancies ($V_O^{\cdot\cdot}$) are compensated by electron carriers as represented by the reaction of Equation (3). When Nb^{+5} is reduced to Nb^{+4}, an electron on ($Nb_{Ti}^{\cdot}$) is formed as a shallow donor in titania [60,61]. Solid oxide fuel cells rely on these defect relationships for conductivity, where defects are more mobile at higher temperature. At lower temperatures, defects may become quenched in the lattice and considered as a quasi-equilibrium that can contribute to new mobility states though bulk diffusion is reduced [62–66]. Only a few other stable elements with higher oxidation are suggested as donors in titania; among these are Nb (V), Ta (VI), and W (VI) oxides found at high potentials ~1 V and in very low pH values often found in electrochemical cells with acidic electrolytes based on proton exchange [28]. Importantly, the oxides of positive transition metals have a tendency to form oxygen vacancies and hydroxides at their surface when reduced through strong interactions with more electronegative metal clusters deposited on them [67]. Substitution limits for

dopant cations depend on their ability to fit into the lattice of the host crystal. The observed coordination with oxygen in TiO_2 is 6 and ionic radius about 0.61 Å, where that of the closest possible donors are Nb^{+5}, Ta^{+5}, and W^{+6} with 0.64, 0.64, and 0.60 Å radii according to the *Handbook of Chemistry and Physics* [68]. These dopant cations can provide for the optimum replacement solubility while inducing only minimal strain in the crystalline lattice. In mesoporous titania films, it was shown that 20% of Ti can be replaced with Nb for very low electrical resistivity [69]. Furthermore, concentrations >25% were successfully included in anatase titania that were stable during an insulator-to-metal transition [70]. Even low level doping in rutile of <1% Nb substitution provided for substantial band gap narrowing and formation of intermediate energy states including shallow donors [71,72]. Crystalline structure and processing conditions are clearly important to Nb inclusion in the phases of titania and its electronic properties. A substitution of 10% Ti with Nb was chosen for this study, but it has been suggested that the other oxides and dopant combinations could also be used in effective electrocatalysts [73–77].

$$Nb_2O_5 \xrightarrow{2TiO_2} 2Nb_{Ti}^{\bullet} + 4O_O^X + \frac{1}{2}O_2 + 2e^- \quad (2)$$

$$O_O^X \rightleftarrows V_O^{\bullet\bullet} + 2e^- + \frac{1}{2}O_2 \quad (3)$$

There are many descriptions of the interaction from Pt deposited on titania present in the literature, especially for catalysis. Tauster notoriously reported a loss of H_2 and CO chemisorption for these supported catalysts on TiO_2 when heated in a vacuum or reducing atmosphere above ~300 °C; this was attributed to the accumulation of electrons from titania at interfaces with Pt that can result in a rapid surface diffusion of Ti^{3+} cations around the noble metal islands at this temperature [78,79]. Encapsulated Pt catalysts were rendered inactive after this conversion due to a dubbed strong metal-support interaction and loss of specific adsorption. Heating in low oxygen pressure causes more electropositive transition metals to encapsulate islands of electronegative metal clusters made of noble group elements on the oxide surface through charge transfer and interfacial reactions that align their Fermi levels and minimize surface energy [67,80–82]. Without chemisorption of H_2 or CO reactants, catalysis is not really possible. However, a beneficial catalytic property from the class of materials that demonstrate strong metal-support interactions can still be realized when prepared at ideal conditions that limit encapsulation [81]. Oxygen vacancies formed in the reduced metal oxide phase near interfaces with the catalyst can provide an important contribution to the bifunctional mechanism while acting as an extension of the active surface in oxidation of CO [83,84]. Interaction of titania with supported Pt has been used in a number of other catalytic reactions (e.g. water-gas shift) where CO adsorption, vacancy formation energy, and electronic interactions have been modeled [85–89]. Interfaces formed with the metal are seemingly important and substantial Schottky barriers are known to form in Pt @ titania where these surface charges accumulate. Related phenomena have been referred to as catalytic nanodiodes and also used for CO oxidation reactions [90,91]. Electrocatalytic oxidation studies for 10% Nb doped anatase and lightly reduced versions of this titanium oxide phase (i.e. $TiO_{2-\delta}$) exemplified better performance and stability than its rutile, undoped, or Magnéli phase counterparts in electrochemical tests [92–96]. These results have also indicated effective alcohol oxidation in the anode where CO is formed as an intermediate in the reaction. Although metallic support conduction is not necessarily required for electrocatalysis, use of dielectric oxides and resistive materials should be minimized. Addition of a carbon component is probably still imperative for improving conductivity and limiting the use of highly crystalline and wide band gap oxides that behave like semiconductors.

Carbon is the most commonly used Pt electrocatalyst support. Unfortunately, carbon can be corroded at low standard potentials; although, the kinetics of oxidation are moderate until conditions become more severe such as those sometimes found in electrochemical cells [23]. The structure of carbon and its surface functionalization have important implications on its applicability in the electrode as well its corrosion resistance [97–99]. Graphitized forms of carbon in the support have been shown to be more stable in these applications than carbon blacks [100–102]. Though, Pt catalysts pose another dilemma because they also facilitate carbon corrosion and bond relatively weakly through functionalized surfaces [103]. CNTs have several attractive attributes which start with their strength, high surface to volume ratio, and improved corrosion resistance, making them a good candidate for graphitic carbon in the electrode as long as catalysts can be attached [103–106]. Strong mechanical properties can prevent electrode structure from collapsing and provide a percolating network along axial directions to maintain diffusion paths with an open porosity [107–110]. In CO tolerance, similar graphitized forms of carbon with oxygen functionality on their surface were shown to have a high activity and used as guides in our design [104,111,112]. The defect sites in carbon act as decoration centers for the metal oxide and catalyst [51,113]. Multi-wall CNTs are known to also exhibit some semiconductor behaviors, but inexpensive commercial versions possess satisfactory electronic conductivity and were chosen as a representative carbon platform in the foundation of composite supports for this research. It is purported that advancements made in this area will be reinforced by a simplified approach for material synthesis and electrode fabrication to demonstrate the support concept which may also serve as a case for further development in related electrocatalysts.

2. Experimental

2.1. Carbon nanotube composite supports

Multi-wall CNTs of 8–15 nm O. D. × 10–50 μm length (Cheap Tubes Inc.) were first oxidized in a mixture with equivalent volumes of concentrated nitric (70%) and sulfuric acid (96.5%) for 3 h at 80 °C to functionalize their surfaces with oxygen groups and remove impurities. Oxidized CNT solids were washed thoroughly with de-ionized water and separated with porous polytetrafluoroethylene (PTFE) filters before drying. Functionalized CNT were ultrasonically dispersed in anhydrous isopropanol solvent before adding precursor amounts of titanium (IV) isopropoxide and in some cases niobium (V) ethoxide solutions (99+%) to reflux under N_2 purge gas at 80 °C for 3 h in a modified sol–gel process [113]. De-ionized (DI) water was added slowly to promote hydrolysis, condensation, and growth of metal oxides on CNTs. Reflux was removed and evaporation of remaining solvents was necessary to collect resulting solids. All support powders were then calcined in N_2 at 450 °C for 2 h to induce ordering and phase transformation. Two different loadings of titania were initially compared by varying ratio of carbon to titanium (or niobium) precursors with atomic proportions of [Ti:C] at [1:10] and [1:100]. The Nb doped titania target was 10% atomic substitution for Ti in the oxide. Three support formulations were prepared to form electrocatalysts: a carbon only control with oxidized CNT, a composite from TiO_x-CNT, and Nb doped titania $Ti_{0.9}Nb_{0.1}O_x$-CNT, where $x \approx 2$ [114]. For simplification, titania and Nb doped form are just denoted as TiO_x and $TiNbO_x$ in the remainder of the publication.

2.2. Electrocatalyst preparation

The deposition of Pt on composite supports was carried out by a microwave-assisted polyol reduction method. The catalyst supports were first ground into fine black powders that were dispersed by an ultrasonic probe (Sonics VCX 750) in ethylene glycol before choloroplatinic acid hexahydrate (8% wt. $H_2PtCl_6 \cdot 6H_2O$) was added to prepare electrocatalysts with projected yields of ~20% Pt mass. The pH of solution was then adjusted past the isoelectronic point and above pH 9 by adding 1 N NaOH dissolved in ethylene glycol to promote Pt nucleation. After stirring, mixtures were rapidly heated in a 1100 W commercial microwave oven (GE) on 60% power setting for 60 s to reach a critical temperature of 140 °C where growth of Pt nanoparticles on the catalyst support is stimulated [115]. The resulting suspensions were again separated by vacuum filtration and the remaining black solids were washed with acetone and then DI water before drying and finally refining size of agglomerations with basic mortar and pestle technique. These composite materials were characterized and used as subjects of electrode testing. The three functionalized electrocatalysts are labeled Pt-CNT, Pt-TiO_x-CNT, and Pt-$TiNbO_x$-CNT.

2.3. Ultrasonic ink processing and electrode fabrication

The resulting electrocatalysts were dispersed into an ink with ionomer and solvents to deposit directly on polymer electrolyte membranes. After weighing the catalyst powders, a few drops of water saturated solids before they were submersed with isopropanol in 20 mL vials. A suspension of the ionic polymer, Nafion® DE-521, was added to equate 20% of solid mass formulation in the electrode. Electrocatalyst inks were then mixed by ultrasonic horn for at least 15 min before being loaded into a syringe used in the sprayer. An automated ultrasonic spray process (Sono-Tek Exactacoat system with an Accumist 180 kHz nozzle) was used to deposit inks directly on substrates, Nafion® NRE-212 membranes in this case [116]. Membranes were placed above a platen heated to 100 °C for accelerating solvent evaporation. A raster pattern was used on square template to obtain MEAs with 25 cm^2 active area and 0.3 mg_{Pt} cm^{-2} loading in the anode. The opposite side was coated with Pt black (Johnson-Matthey HiSPEC 1000) with 2 mg_{Pt} cm^{-2} loading by a specialized process which also served as a reference electrode [117].

2.4. Membrane electrode assembly and cell construction

MEAs were sprayed and then dried prior to pneumatic hot press at 130 °C for 5 min under 3250 kPa pressure. The pressed MEAs were soaked in 0.5 M sulfuric acid for one hour at 80 °C to protonate ionomer electrolyte before thorough rinse in DI water. Test cells were built with a set of SGL Carbon 10 BC gas diffusion layers (GDL) and 254 μm thick PTFE gaskets to impose a 33% pinch of GDL by applying 9 N·m torque to tie bolts in cell hardware (Fuel Cell Technologies, Inc.). Cells were assembled in graphite flow plates with triple serpentine flow channels, and connected to a fuel cell test station (Scribner 840) which feeds pure gas (H_2 or N_2) at controlled temperature and water saturation to the cell. An external humidifier and flow controller (MKS) were used to humidify and control H_2 mixed with 100 ppm CO (Praxair) fed into the cell. The experimental test setup is shown in Fig. 1.

2.5. Electrochemical diagnostic tests

Several electrochemical experiments were carried out to compare performance of cells with different anode electrocatalysts. The active electrochemical surface area was measured by cyclic voltammetry (CV). CO tolerance of the anodes was evaluated by both chronopoteniometry and chronoamperometry experiments on cells operated in the hydrogen pump mode. CO stripping voltammetry was used to compare oxidation behavior during contaminant removal. Electrochemical impedance spectroscopy (EIS) technique was applied to assess charge transfer resistance. Tests were carried out with a potentiostat/galvanostat (Gamry Reference 3000) coupled to a power booster (Reference 30k). Flow rates for the fuel and purge gas were all set to 250 mL min^{-1}, unless otherwise noted. The Pt black cathode is supplied with clean H_2 and also serves as a pseudo-reference electrode. In hydrogen pumps, anodes were exposed to flows of the contaminated H_2 to provide the source of protons. Cell temperature for all experiments was set at 75 °C with feed gases fully humidified to 100% relative humidity (RH).

Initially, potential cycling was applied to all electrodes from 0.05 to 1.2 V at 50 mV s^{-1} for 500 cycles to accelerate aging during a break-in process. CO stripping was completed by the same potential cycle parameters. Working electrodes were under constant exposure to 100 ppm CO in H_2 for at least 30 min prior to removal. For accurate peak determinations, H_2 pump anodes were then purged with N_2 for >15 min to flush excess CO and provide ample time for the open circuit voltage to stabilize in the cell. Chronopotentiometric tests with galvanostatic current density from 3.125, 6.25, 12.5, 25, 50, to 100 A m^{-2}_{Pt} were supplied at constant stoichiometric H_2 flow rate of 10 normalized to the Pt active area. Voltage measurements were collected over a period of at least 2500 s and up to 1 h at lowest current density. Adsorbed CO in the electrode was cleaned up in between tests by the stripping procedure before repeating tests at next highest current density setting. Chronoamperometric tests were applied at 25 mV potentiostatic for 10 min under constant flow rates normalized to the electrochemically active Pt surface area of catalysts. Current was recorded during this span which was sufficient to reach a CO saturated condition and stabilize cell performance. EIS also complemented the potentiostatic condition from the previous step using scans from 2500 to 2.5 Hz and 5 mV perturbations with successive

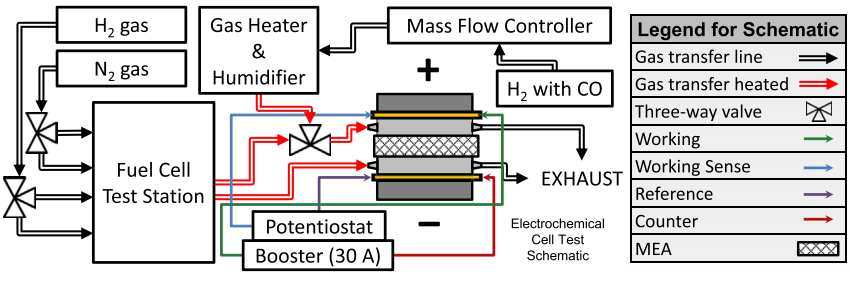

Fig. 1. Schematic of electrochemical cell test designed to characterize anodes (+).

spectra at exact intervals of 1 min for the first 10 min of exposure to CO. The time dependent and steady state electrochemical behavior is presented in the results and discussion.

2.6. Materials characterization

The prepared materials were characterized by a suite of analytical techniques. Raman spectra of the catalyst supports were obtained by a Horiba LabRam-HR system with a He–Ne laser (λ = 633 nm). Powder X-ray diffraction (XRD) patterns were collected by a Rigaku Mini-Flex instrument with CuK_α radiation and D/teX detector. Scanning transmission electron microscope coupled with energy dispersive X-ray spectroscopy (STEM/EDX) on a Hitachi S4800 and a high resolution transmission electron microscope (TEM) on a Hitachi H9500 were used to image the electrocatalysts. X-ray fluorescence (XRF) by Fischer XDAL instrument was used to analyze the Pt loading in the MEA. X-ray photoelectron spectroscopy (XPS) using a Kratos Axis Ultra DLD equipped with a monochromated Al K_α X-ray source and hemispherical analyzer probed electronic interactions. Binding energy was calibrated using an Ag foil with Ag $3d_{5/2}$ set at 368.21 ± 0.025 eV while the source was operated at 15 keV and 120 W.

3. Results and discussion

3.1. Material characterization of composite supports

The first characterization by XRD aimed to identify the structure of phases in composite supports. A spectrum from titania and CNT with an atomic ratio of Ti to C [1:10] showed peaks representing the formation for anatase phase from TiO_2 with well-defined crystallinity on carbon supports at this concentration. The average anatase (A) crystal size was under 10 nm from Scherrer equation applied to A (200) and (204) peaks which have been labeled in Fig. 2. When the ratio of titanium to carbon [Ti:C] was decreased by an order of magnitude for an estimated yield [1:100], the oxide structure was obscured due to reduced crystallinity and mass accounting for $\lesssim$ 5% of total [118,119]. This construction was prepared by the same procedure, but was more disordered with only partial coverage and resultant spectra dominated by the features of graphitized carbon (C) [45,113,120,121]. A significant improvement in performance from the [1:100] atomic ratio of oxidized metal to C resulted in this parameter being held constant for supports used in electrochemical cell test results presented later in the publication.

A confocal Raman spectroscopic investigation was used to probe the nature of metal oxides joined to CNT and confirm their presence. The six active vibrational modes of anatase titania are observed below 700 cm^{-1} from composite supports plotted in Fig. 3 [122]. A decrease in all peak intensities is noticed for [1:100] ratio with lesser Ti content. The most intense peak is attributed to the lowest frequency for E_g mode while the smaller signal contribution can be related to a reduced degree of crystallinity [123]. Moreover, this main peak has tendency to blue-shift and broaden asymmetrically towards higher wavenumber due to decrease of particle size, oxygen vacancy formation, interfacial surface vibrations, and photon confinement effects [124]. The resulting main E_g peaks in supports have been identified at 159.4, 160.5, and 161.3 cm^{-1} with Nb doped titania showing the lowest intensity and largest Stokes shift. It has elsewhere been reported that additions of Nb in titanium dioxide increase the temperature of phase transformations and retard its grain growth [69,125,126]. A decreased degree of order in the doped sample is the probable result. Presence of features in composites with peaks near 1350 cm^{-1} and 1600 cm^{-1} are associated with the graphitic and disordered carbon bonding vibrations of multi-wall CNTs which do not differ substantially [127].

3.2. Material characterization of electrocatalysts

After polyol deposition of Pt on supports, XRD analysis was performed again to observe growth of Pt catalyst nanostructures in Fig. 4. Similar crystalline peaks were observed in all three electrocatalysts, but there were differences in the size of catalysts on supports. From interpretation of Pt (220) facets, the average size of catalysts decreased from Pt-CNT > Pt-TiO_x-CNT > Pt-$TiNbO_x$-CNT with values of 8.15, 4.99, and 4.89 nm at peak centers identified for 2θ values of 67.62, 67.88, and 67.80, respectively. Composite supports seem to improve distribution and limit the growth of catalysts to a much greater extent when synthesized under similar conditions [120,128–130]. This may be attributed in part to the interaction between Pt and the electropositive transition metals used in the support. By this rationale, there could be some consideration of Pt size effects since the Pt on CNT grew to a larger diameter. Regardless, the order of size did not directly correlate with their performance, suggesting support specific electrocatalyst effects.

XPS was used to verify the presence of transition metals and the effect on their core electrons after Pt deposition. Peak shoulders and shifts in the positive (oxidation) and negative (reduction) direction of the binding energy (BE) are observed. The BE values

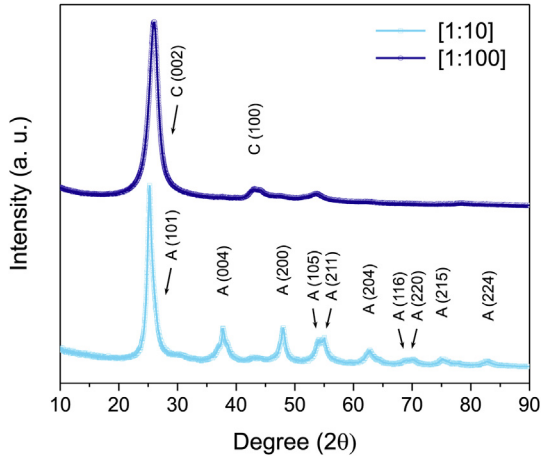

Fig. 2. XRD of Titania-CNT composites.

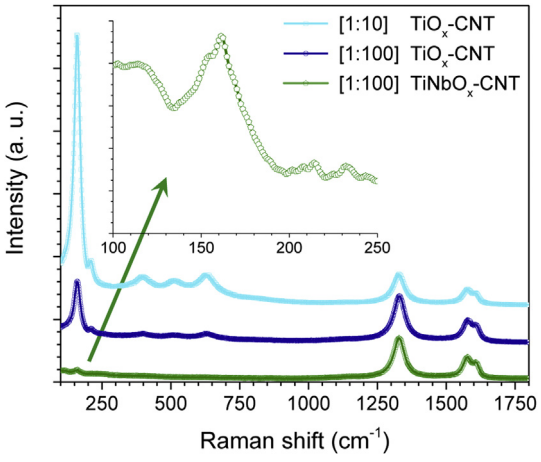

Fig. 3. Raman spectra of composite supports.

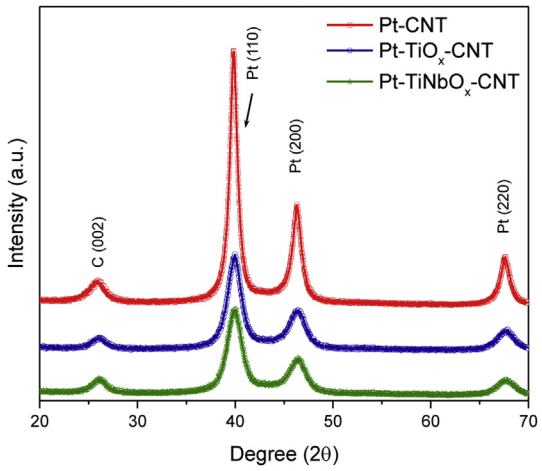

Fig. 4. XRD of electrocatalysts after Pt deposition.

have been referenced to fit the main C 1s peak at BE of 284.6 eV due to various charging effects and all intensities have been overlaid for the sake of comparison purposes. As shown in Fig. 5, a reduction shift in BE of core Ti 2p and Nb 3d orbitals for Pt electrocatalysts (—*—) is seen when compared to supports (—) only. Presence of reduced Ti (III) and Nb (IV) valence states in metal oxides are more apparent after Pt deposition by formation of shoulders and asymmetric artifacts extending to BE values below support only spectra [69,72]. The added signal noise in the plots with Pt is another indication that much of the oxide surface has been covered by catalysts. Interfaces formed with Pt seemingly increase the concentration of reduced transition metal species in this instance.

A cooperative interaction between Pt, the metal oxides, and multi-wall CNT may further be realized by examination of O 1s peaks. As shown in Fig. 6, peaks centered around 530 eV arise in composite supports shown in (b) and (c) which do not even exist for the CNT control seen in (a). This peak with the highest binding intensity is attributed to the M—O bond. In composites with titania, it becomes considerably diminished after Pt deposition. This is a suspected result of the interaction between Pt and Ti or Nb along with the essential creation of oxygen vacancies. The surface oxygen vacancy has been found as a nucleation center for growth of Pt, providing for the strong interaction [48,128,131,132]. Addition of a donor dopant can assist in the creation of more oxygen vacancies that are stabilized by the Pt deposition. Oxygen vacancies or dangling bonds can be healed by dissociated hydroxyls near catalyst interfaces to form M—OH species on the oxide surface [38,133]. Several reports have also found this to be beneficial in ORR where the metal oxide could be assisting transfer of hydroxyl intermediates from the catalyst, a rate limiting step of that half-reaction [74,76,84,134]. In the bifunctional mechanism for CO oxidation in the anode, metal oxides are expected to facilitate supply of hydroxyl groups to the catalyst reaction site.

The Pt 4f peak from XPS also tells us important information about the properties of the electrocatalyst. Several XPS studies of Pt on titania catalysts prepared in a similar fashion to this paper that were also corrected to C 1s found BE values reduced by some extent when 4f plots were compared to a control and this was credited to a strong metal-support interaction [51,74,134–136]. In this study, titania electrocatalysts also revealed reductive shifts for Pt doublets when referenced to the C 1s peak. However, due to charging within varying functionalization of carbon surfaces and increased interfacial contact of Pt with metal oxides in composites, the 4f spectra

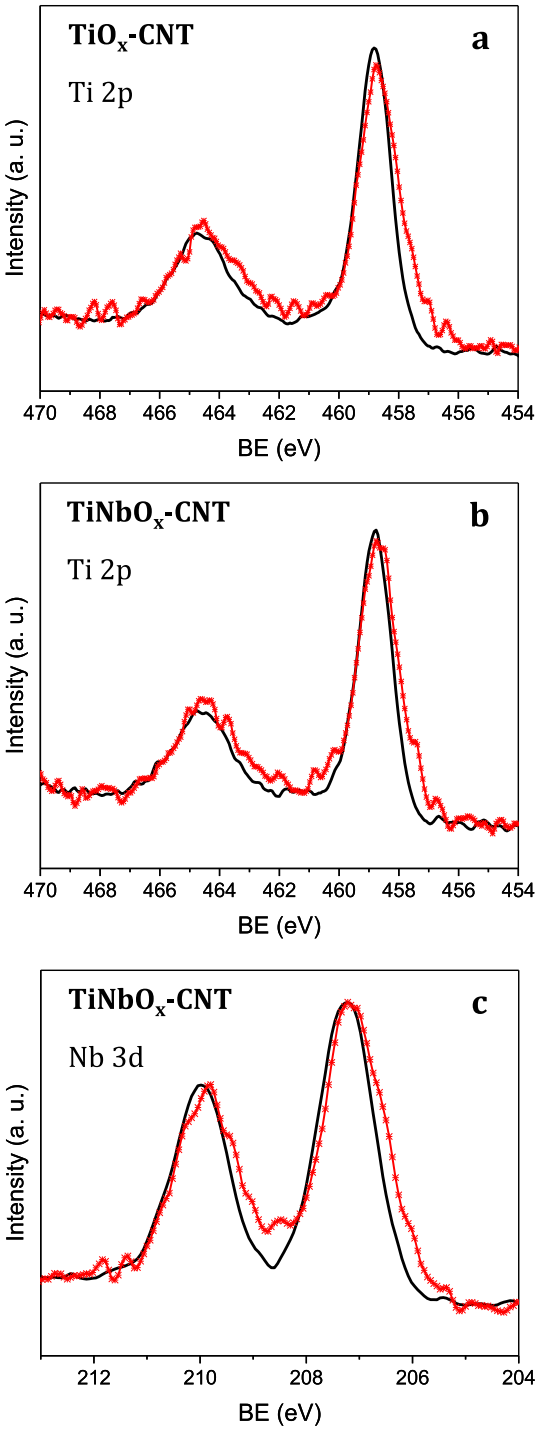

Fig. 5. XPS analyses show the transition metal spectra in composites before (—) and after (—*—) Pt deposition.

were re-plotted with reference to their valence band edge aligned at 0 eV and superimposed in Fig. 7. In this comparison, a positive shift >0.1 eV in BE was measured for Pt-TiNbO$_x$-CNT from the Pt-CNT control. Shallow Nb^{4+} donors in TiNbO$_x$ probably pin the Fermi level of the metal oxide further from its valence band edge, allowing some nonbonding electrons to more easily enter the metal. These effects can be attributed to the formation of a Schottky junction which results from alignment of energy levels at the interface and the differing work functions in metal—metal oxide composites. Deeper defect states from Ti^{3+} are known to reside

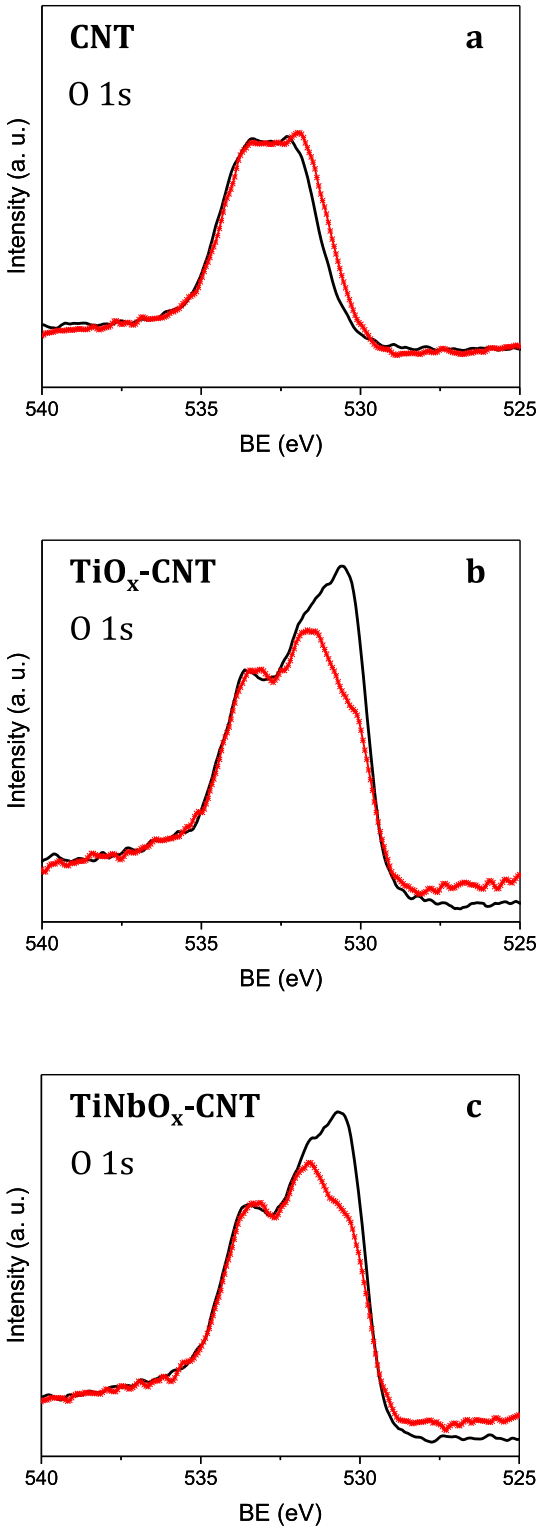

Fig. 6. XPS of O 1s in (a) CNT, (b) TiO_x-CNT, and (c) $TiNbO_x$-CNT supports before (—) and after (—*—) Pt.

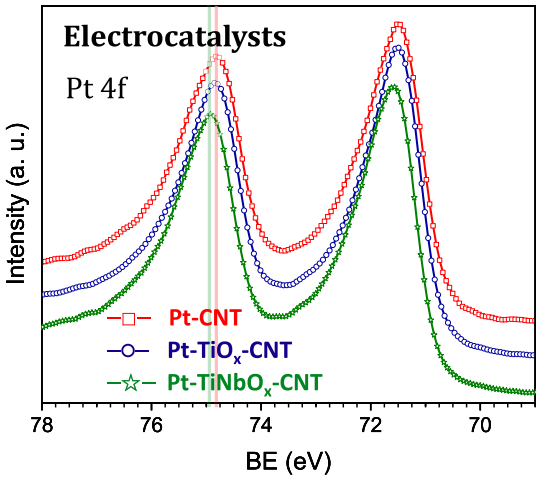

Fig. 7. XPS spectra of Pt 4f peaks for all electrocatalysts.

closer to the middle of the titania gap, resulting in only mild Fermi level shift of Pt at the TiO_x-CNT junction. Several other strong-metal support electrocatalysts with similar compositions also saw positive or only minor shift in BE when contrasted by this method to a Pt control [46,120,137]. In the anode, a small shift in the Pt electron energy level probably does not significantly change CO adsorption properties. Advantages for CO tolerance thus extend to the nature of its interface with support materials.

A sequence of TEM images show increasing magnification of a Pt-$TiNbO_x$-CNT electrocatalyst. Pt nanoparticles (dark) are supported on Nb doped titania and CNT presented in Fig. 8. The TEM images were zoomed in on a region where some catalysts are nicely distributed on the composite support, but others are not. The mean of Pt particles was confirmed under 5 nm from particle counting statistics. In comparison, Pt-CNT electrocatalysts demonstrated worse agglomeration of Pt and more irregular distribution of attachment. Evidence of the titania phases is not readily apparent in composites, another indication of their small size and more disordered nature. A high resolution TEM study found the metal oxide in hybrid support design with a disordered structure around Pt interfaces provided for improvements to activity in methanol oxidation and CO tolerance [134]. Other reduced metal oxides like ceria supported Pt electrocatalysts also found amorphous arrangements of defected oxide around catalyst interfaces with the best oxidation reactivity due to formation of Ce (III) in CeO_2 [30,138]. One recent report on doped titania supports proclaimed the origin of their catalyst enhancement for ORR was derived from the resultant strain induced in the Pt lattice bonded to the crystalline metal oxide [135]. However, several other examples such as amorphous niobia used in supports for Pt electrocatalysts found high activity and stability in both electrodes [139–144]. It seems that the low degree of crystallinity for metal oxides in this work and that found by others would also suggest that the oxide effect extends beyond the Pt metal lattice by altering charge transfer reactions in the support. Specifically, the formation of hydroxyl groups near the catalyst interface can play an important factor in its activity.

STEM (upper left) coupled with energy dispersive X-ray (EDX) spectroscopy (in color) reveals presence of all the metals and their corresponding distributions in Fig. 9. Metal oxides are evident in composite supports and it seems that the dopants were well mixed into the titania matrix. All of the supporting images consistently show that the Pt nanoparticles have a tendency to deposit on or near the metal oxide phase in the composite support, providing further evidence that noble metals are anchored through strong interfacial junctions [50,145,146]. Compositions of the metal oxide were more apparent when coupled with EDX analysis than found with the high resolution TEM images alone. Nb content was measured in this sample and several other images at concentrations $\geq$10% dopant fraction in titania. Additionally, in all samples the total atomic fraction of transition elements (Ti and Nb) was less

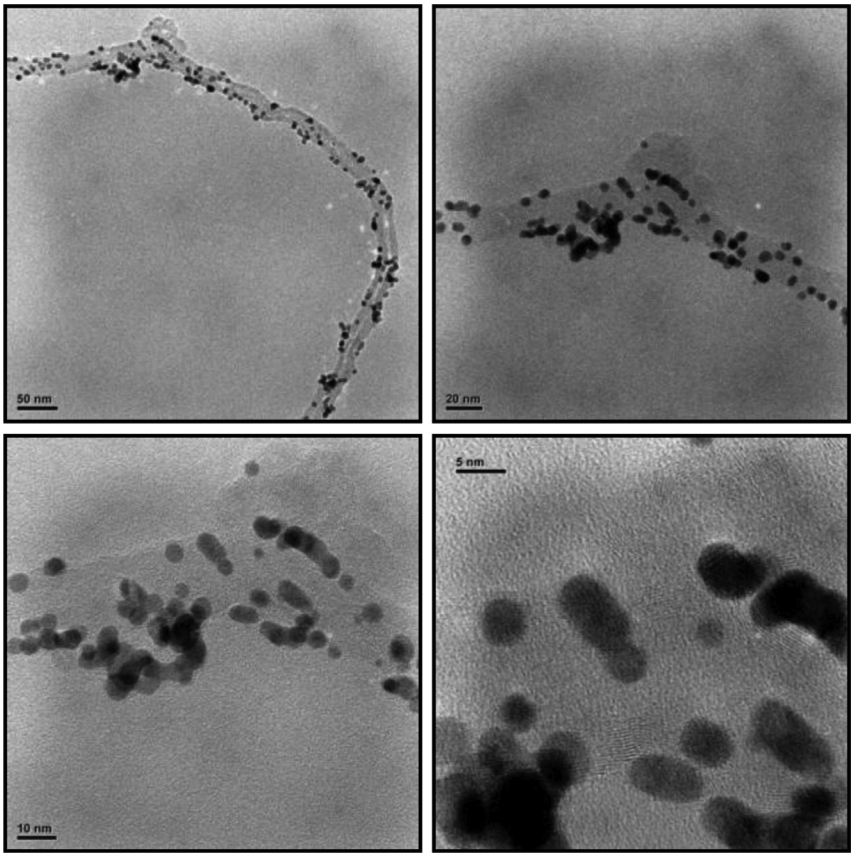

Fig. 8. High resolution series of TEM images at increasing magnification for Pt-TiNbO$_x$-CNT.

than half the Pt atomic content. It is expected that these proportions could have been optimized for further improvements in electrochemical performance. Regardless, a proof of concept can be recognized by this composite arrangement.

3.3. Electrochemical characterization of working electrodes

Initial electrochemical tests indicated that cell electrocatalyst area was evolving from the effects of potential cycling applied for CO stripping cycles. To stabilize electrodes and make consistent measurements, they were all subjected to a series of 500 potential cycles up to 1.2 V before further tolerance testing. This process accelerated cell aging to break-in catalysts. After cycling, all three electrocatalysts demonstrated stable electrochemical performance. The CVs before and after the procedure are compared in Fig. 10. The reference electrode was comprised of unsupported Pt black under clean hydrogen. A clear trend in the order of active area preserved from this test shows Pt-TiNbO$_x$-CNT had the best stability after

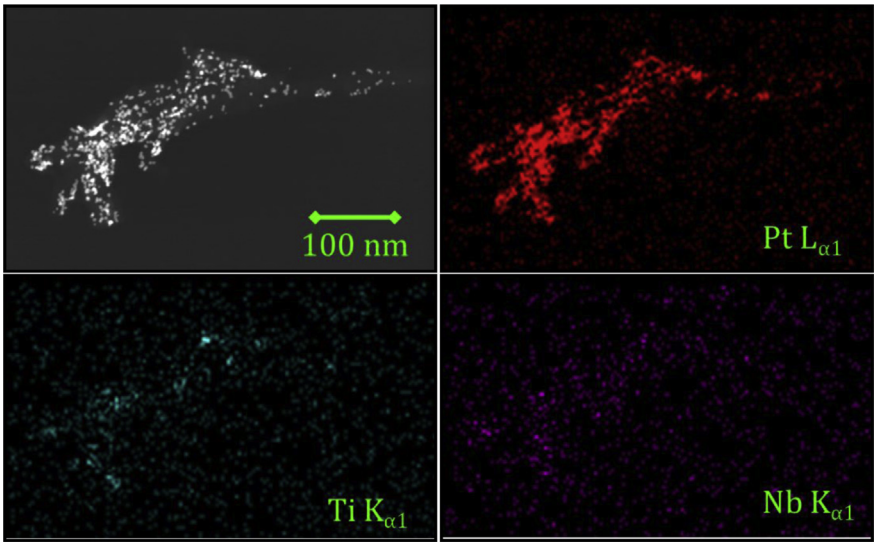

Fig. 9. STEM/EDX of Pt-TiNbO$_x$-CNT.

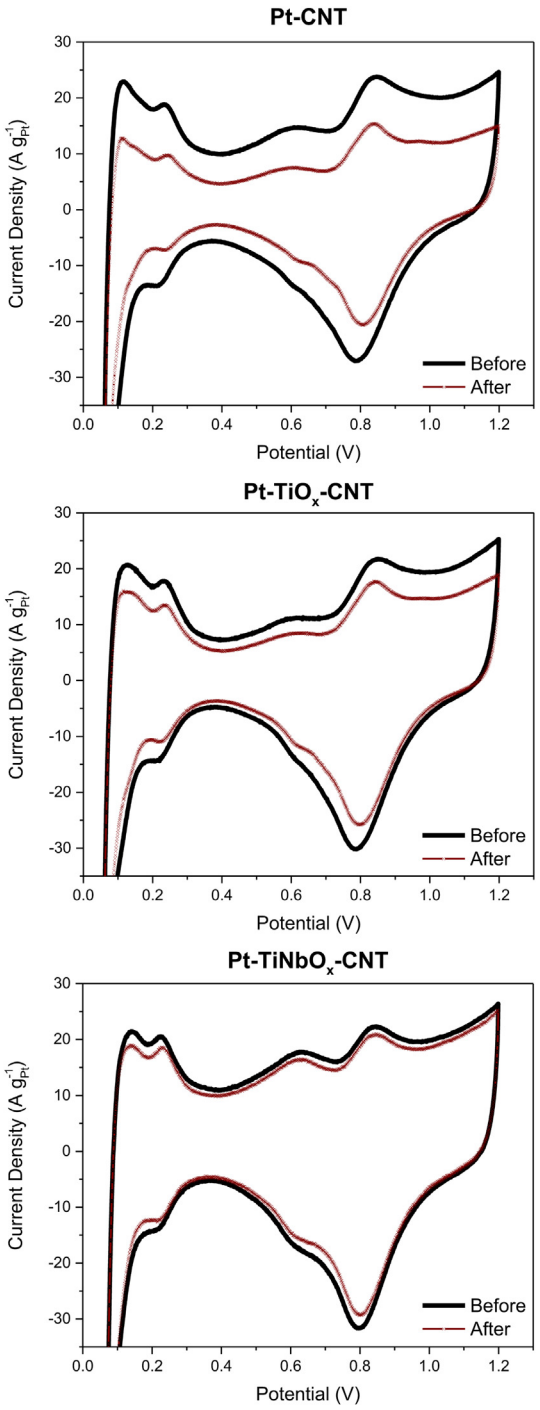

Fig. 10. Cyclic voltammetry shown before and after break-in procedure.

break-in cycling was completed to simulate stressors during aging. Notably, Pt-TiNbO$_x$-CNT also had the widest double-layer of all three working electrodes. The hydrogen underpotential deposition (UPD) from the reversible reaction before and after cell break-in are shown in Table 1; UPD features were integrated after subtracting double-layer capacitance to determine the total active electrocatalyst surfaces based on the area specific conversion of 210 μC cm^{-2} [147,148]. Better catalyst utilization from ultrasonic processing has been measured for commercial catalysts by this automated deposition procedure that provides for uniform, thin, and reproducible electrodes [116]. However, electrocatalysts

Table 1
Summary of electrocatalyst utilization before and after break-in cycling.

Pt features	Pt-CNT	Pt-TiO$_x$-CNT	Pt-TiNbO$_x$-CNT
Utiliz. Before	18.5 m^2 g$^{-1}_{Pt}$	21.2 m^2 g$^{-1}_{Pt}$	15.3 m^2 g$^{-1}_{Pt}$
Utiliz. After	11.2 m^2 g$^{-1}_{Pt}$	16.9 m^2 g$^{-1}_{Pt}$	13.6 m^2 g$^{-1}_{Pt}$
Remaining	60.7%	80.0%	88.6%

synthesized in our laboratory can be fairly compared by this process. Based on areas remaining after break-in, stoichiometric flow rates and current densities were kept proportional to active Pt surfaces for comparison purposes.

CO stripping peaks in Fig. 11 were collected after extended exposure to the CO contaminated fuel. Peak maxima from anodic strips were measured at 591, 607, and 616 mV corresponding to the order of activation for the Pt-TiNbO$_x$-CNT, Pt-CNT, and Pt-TiO$_x$-CNT electrocatalysts, respectively. Interestingly, the CO tolerance and stripping behavior of Pt-CNT improved from the initial condition; specifically, the order of activity for the CNT only support surpassed that of the TiO$_x$ composite [149]. Although even higher temperatures would have improved tolerance, increasing to 75 °C offered satisfactory activity to make appropriate comparisons. Cell temperature can have an impact on all the reactions, including corrosion. Faster degradation and loss of active Pt surfaces on CNT leads to formation of carboxyl and hydroxyl groups during support oxidation which may also assist their tolerance [23,111]. Furthermore, size effects and faceting of Pt can improve specific activity in oxidation reactions and could have become a factor [112,115,150–152]. Irrespectively, the order of catalyst size, utilization, and/or stability did not directly correlate with CO tolerance found in this study, further suggesting catalyst support contributions.

At galvanostatic conditions, the potential can be measured over time (chronopotentiometry) while subject to a stoichiometric flow of contaminated H_2. This hydrogen pump mode is one of the best ways to test for CO tolerance because the dynamic in working electrodes from increases in overpotential are easily observed and attributed to catalyst behaviors. In clean H_2, the cells displayed stable and nearly identical polarization behavior in the pump. When CO is present, potential climbs gradually with time before a sharp transition is observed in each data series shown in Fig. 12. After the transition, the cell potential plateaus as more stable performance is approached. At higher currents, the cell potential can undergo an oscillating behavior after the transition. In the Pt-CNT electrode for example, potential oscillations started during

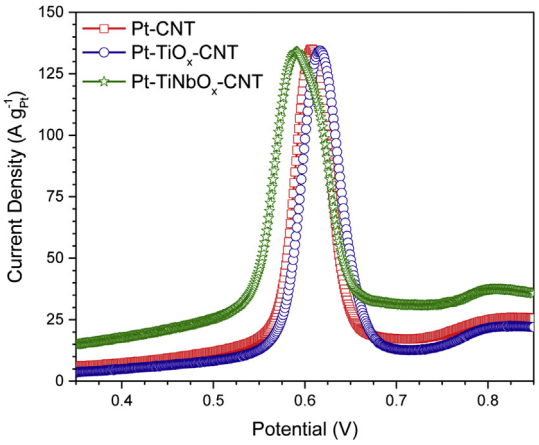

Fig. 11. CO stripping behavior of electrocatalysts.

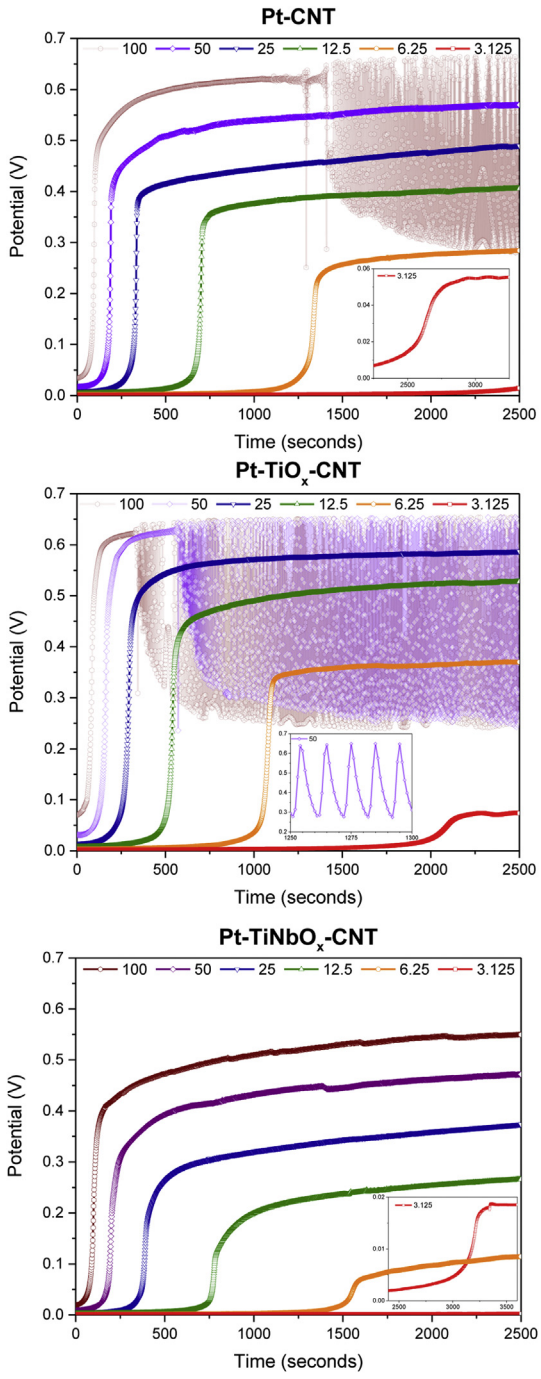

Fig. 12. Galvanostatic responses to H_2 with CO shows change over time via chronopotentiometry.

application of 100 A m^{-2}_{Pt} after about 1250 s. Oscillating behaviors were observed in all electrodes although they did not begin in Pt-TiNbO$_x$-CNT until supplying higher current densities (>100 A m^{-2}_{Pt}) and are marked by transparent plots to prevent overlapping data sets. When the overpotential climbs above the CO oxidation peak, adsorbed CO on the catalyst surface will be oxidized and active sites regenerate, resulting in a reduction of cell potential. However, unreacted CO in the electrode will quickly adsorb again onto active surfaces, leading to another rise in potential before the cycle repeats as seen in magnified inset of Pt-TiO$_x$-CNT at 50 A m^{-2}_{Pt} current density. Similar oscillating phenomena are quite familiar to other types of heterogeneous catalysis and have also been reported in the electrocatalysis literature [153]. These transitions may hold important information and provide valuable insight into the electrode behavior. Performance data recorded after the transitions when CO has covered active surfaces is most telling of electrocatalyst overpotential at semi-steady state.

After surpassing the transition step, the final potential value was recorded at each current density applied. Those points are plotted on a curve in Fig. 13 for comparison purposes and can correlate to differences in catalyst overpotential when CO is present at this fixed concentration (100 ppm) with a stoichiometric flow of H_2. For galvanostatic current of 6.25 A m^{-2}_{Pt}, a reduction of 170 mV compared to Pt-CNT and 256 mV in case of Pt-TiO$_x$-CNT for Nb doped titania support. At 25 A m^{-2}_{Pt}, a savings of 117 mV was measured for Pt-TiNbO$_x$-CNT electrode from Pt-CNT electrode. Essentially, electrocatalysts made from Nb doped titania showed the best CO tolerance by large margins which narrowed at higher current density as cell potentials converged towards the CO stripping peak.

Several interesting trends were observed in the timing of transitional behaviors encountered during chronopotentiometry experiments. The time of transitions was compared by plotting the inflection point in curves of Fig. 14(a) at each fixed current density. Inflections followed nearly perfect hyperbolic relationships. The inset in (a) shows the same relationship, but with the reciprocal of time coordinated to the *X*-axis. Interestingly, the order of the transition times also followed that of activity with an increasing delay in electrode deactivation for Pt-TiNbO$_x$-CNT. Although electrodes can have variations in transport properties, it seems more than coincidental that this also followed the general trend of tolerance. In Fig. 14(b), the rate of the transition step is estimated by the slope (dE/dt) at the inflection. The rate is slower at lower current density for all electrodes. However, there are also variations in rates between different electrocatalysts where transitions grew fastest in Pt-CNT electrodes at higher current. An alteration of specific adsorption properties could affect the time it takes for CO to deactivate all catalyst sites, but it is expected that interfaces with the support play a role in charge transfer reactions that may increase active site availability due to hydroxyl formation in oxides by a mechanism that will be developed in further detail at the end of this discussion.

During application of 25 mV constant potential, current responses were recorded over time (chronoamperometry). Currents were supplied from charged species generated in the anode while CO gradually diffused to catalyst surfaces. Flow rates were also

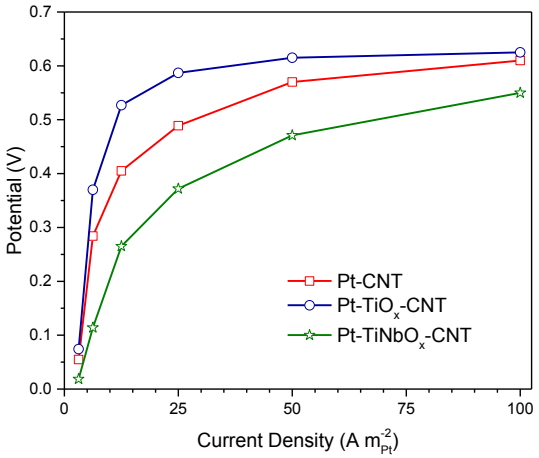

Fig. 13. Cell potential as a function of specific current density applied.

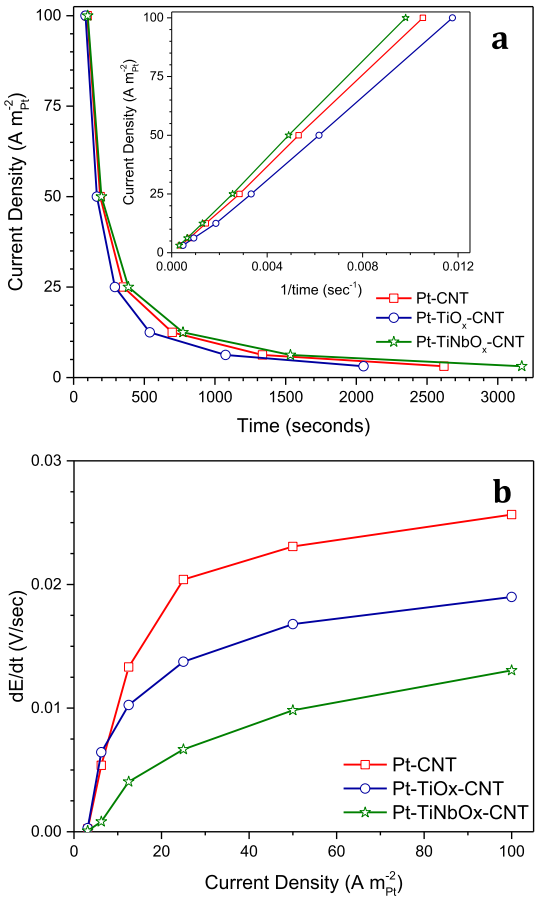

Fig. 14. Characteristics of (a) inflection point in transition and (b) rate of transition vs. current density.

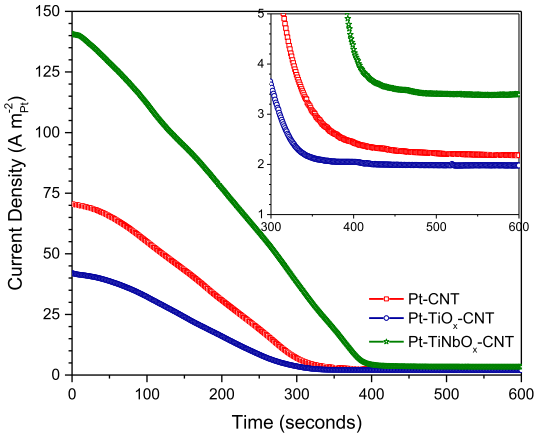

Fig. 15. Potentiostatic condition at 25 mV provides chronoamperometric response.

normal to UPD area and sufficient to provide limiting current at this low potential where adsorption is not significantly affected. During the initial decay of current density, it is perhaps not fair to compare performance due to different stoichiometric reaction values that cannot be controlled unless flow rates are continuously variable. However, after cell currents flatten out to semi-steady state, the response is more equitably compared by a direct relationship magnified in the inset of Fig. 15. For 100 ppm CO in H_2, the cell with Nb doped titania support yielded a current density about 3.5 versus 2.25 A m^{-2}_{Pt} for Pt-CNT, representing a 155% improvement. The same order of tolerance found in chronopotentiometry was also observed during this test.

To compare the time delayed poisoning response of electrodes during potentiostatic condition, an EIS technique was used to observe the loss in activity dominated by charge transfer resistance that results in the growth of impedance arcs during CO poisoning [154]. With otherwise same test conditions described in chronoamperometry at 25 mV, EIS scans were collected at 1 min intervals to show evolution of arcs in Nyquist plots during the cell deactivation in Fig. 16. Impedance plots are zoomed in to focus on earliest stages of development during first 5 min of operation with a high to low scan taken during each minute of this test. At 4 min, the impedance data is noted at the apex and reported as [ω (Hz), Z_{real} (mΩ)]. The highest impedance values were recorded from Pt-TiO_x-CNT at [19.86, 7.62], [31.67, 5.94], to [49.87, 4.83] with the lowest in Pt-$TiNbO_x$-CNT which was also recorded at the highest frequency. The doped composite support electrocatalyst exhibited the most prolonged rise in charge transfer resistance from the CO contamination effects at this condition.

Addition of only a small amount of metal oxides (~5%) to the catalyst support made for a marked contrast in electrode performance. A probable explanation for resulting reactivity differences may simply be attributed to support interfaces with the active catalyst for the improvement in tolerance to CO provided by its design. Lower catalyst utilization measured from UPD in doped titania could in fact represent interfaces where bifunctional reactions are enhanced and hydrogen redox is limited. Oxygen vacancies formed in close contact to catalysts supply a source of hydroxyl intermediates that extend active surfaces for CO oxidation. Strong chemical interactions between the metal and metal oxides result in changes of defect formation energy in the metal oxide. Transition metals at the interface get reduced and this may be more favorable for niobia according to the Gibbs free energy of reaction found in Ellingham diagrams. At higher concentrations, Nb is known to segregate to surfaces of titania during oxidative processes and possibly enrich defects there [70,114,126]. Niobia prefers a higher surface coordination with oxygen than titania cations and may enhance oxygen exchange during surface redox reactions. Nb substitution has also been reported to suppress encapsulation of Pt by Ti suboxides in addition to a having higher oxygen vacancy diffusion resulting from strong metal-support interactions [155]. These metal oxides may partially encapsulate catalysts, but during application of potential, a very stable passivation layer should protect them from more severe oxidative corrosion. Although quantum size effects and interfaces with metals change electronic structure, Nb_2O_5 is known to have a wider band gap than TiO_2 semiconductors. Pseudocapacitive effects from metal oxide redox reactions near the interface with the catalyst may allow them to contribute through the bifunctional mechanism. Semiconductors are perhaps not involved in direct electronic transfer, but could still participate when polarized.

It is not exactly clear what lead to all the trends seen in tolerance, although it may be due in part to the semiconductor like properties of the support. The presence of metal and semiconductor interfaces (i.e. metal oxide or CNT) result in band bending and Schottky junctions or more ohmic like contacts. Heterojunctions found between phases of the electrocatalyst align Fermi levels and potentially shift their energy bands. Point defects from the reduction of metal oxides contribute delocalized electrons and holes. Reduced Ti cations in substitutional or interstitial sites of titania induce deeper mobility states closer to middle of gap that cause it to act more like an ohmic contact when Pt is added [58,88,133,155]. In the case of the Nb doped titania however, the

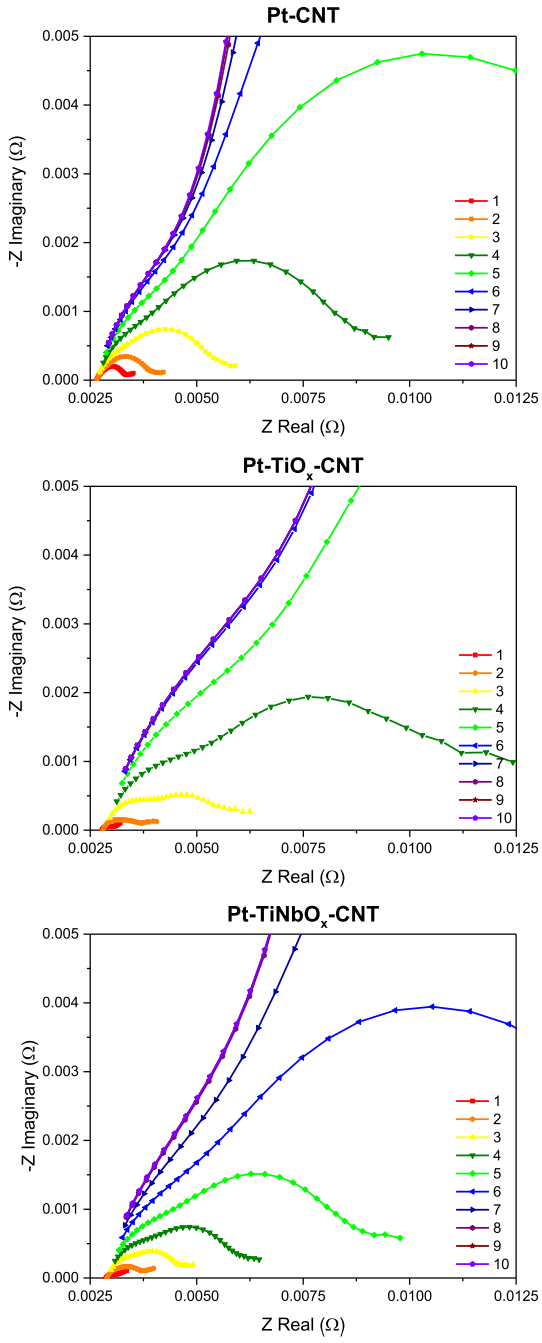

Fig. 16. Evolution of EIS during CO exposure at 25 mV (1–10 min).

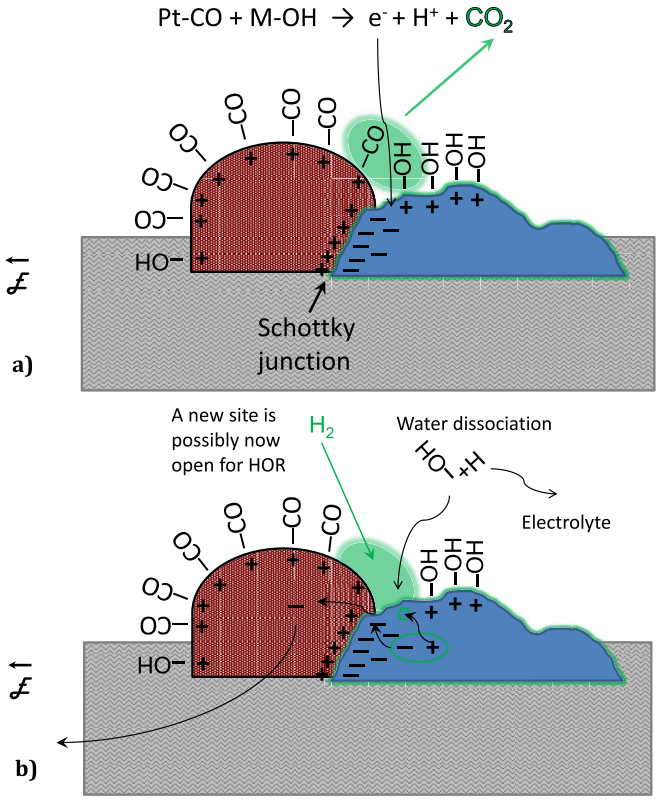

Fig. 17. Schematic of (a) bifunctional mechanism for CO tolerance in poisoned electrocatalysts and (b) separation of an electron–hole pair allows an electron to cross Schottky junction.

Fermi level of the oxide at equilibrium should be pinned closer to the conduction band of this n-type conductor due to addition of shallow Nb^{4+} donor states that can create a useful Schottky barrier. When electrons are taken away and the work function of the metal is increased, more holes are left in the depletion region of the oxide forming a wider space charge layer (i.e. internal field). During this forward bias, a lower activation for excited electrons in the conduction band of the metal oxide will allow them to cross the barrier into the metal, preventing recombination with a hole. Separated charges are more probable to participate in reactions like the formation of reactive hydroxyls at holes or vacancy sites near the surface as depicted in Fig. 17. Formation of Schottky junctions have elsewhere been reported for these metals; in our case, reduced transition metal states seen by XPS suggest they exist here as well. For these reasons, strong metal-support interactions employed in electrocatalysts can also be treated from the perspective of semiconductor principles. Defects stabilized at junctions allow them to become involved in reversible electrochemical reactions. However, it can become difficult to discuss point defects and semiconductor behavior from nanostructured and amorphous oxides. A better comprehension of catalyst-support interplay and underlying electronic structure effects will be expected to help bridge barriers and tune energy gaps between phases that lead to further advances.

There may also be several reasons why the composite supports with titania were more stable than the CNT only counterpart. In general, the presence of catalysts on support chemistry and its effect on stabilizing defects is seemingly important. In widespread reports on electrocatalysts, strong interactions from catalysts on stable supports like titania have boosted their corrosion resistance. The immunity to break-in and operational conditioning from composite titania supports presented here may also be due to its Schottky junction. Excited electrons tunneling into the electrocatalyst from the oxide would protect electrocatalysts as the metal oxide passivates. In this case, titania could be acting like a gated interface to limit corrosion once electron access gets cut off. Water dissociation on titania can also promote hydroxyl formation and facilitate oxygen coverage on catalysts during passivation. A wider space charge layer from the doped oxide is proposed to have better buffering capacity. Titania bonds strongly to the catalyst through these interfaces, preventing its diffusion and detachment from the support while limiting carbon corrosion in those regions. More systematic and exhaustive accelerated degradations tests would help elucidate specific advantages from metal oxides used in related electrocatalysts. There have been reports of non-Pt

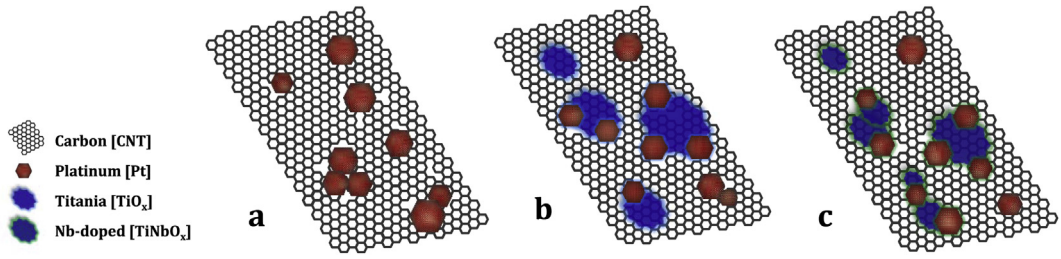

Fig. 18. Representative construction of electrocatalysts (a) Pt-CNT, (b) Pt-TiO$_x$-CNT, (c) Pt-TiNbO$_x$-CNT.

electrocatalysts such as those from heavily reduced Group IV-VI transition metal oxides (including titania) that provide high electrocatalytic reactivity, but their active sites are much further from thermodynamic equilibrium and subject to irreversible oxidation. Simply from the consideration of metal oxide defects, acceptors are preferred at higher oxygen pressure while hydrogen and reducing gases used in the anode favor donor formation. Similar to tolerance though, there are many factors to consider in stability. Integrating metal oxides into the support can have a synergistic effect on electrocatalyst performance and durability, but further developments are needed to derive the best arrangements and compositions.

Relationships described in this set of materials result from their collective and varied properties. The suspected complexity expected for composites is depicted in Fig. 18 to help to visualize some of their interactions. The phases of titania are formed at defects on the surface of oxidized CNT supports to synthesize composites in the first step of the sequence. Blue patches represent fine anatase crystals and other disordered oxide arrangements with a higher concentration of defects near their boundaries. Although Pt catalysts can bond directly through defects in CNT, a stronger interaction with the metal oxide provides a favorable attachment point to form a secure bridge with the support. Triple junctions arise between the metal, metal oxide, and CNT framework. Titania composite supports grow smaller Pt crystals with better distribution. Some of the Pt may become partially covered by the oxide, but this can have advantages including the extension of active bifunctional surfaces. The coverage of Pt by the metal oxide and the nature of their interfaces affect the oxide properties. In the case of doped titania, green borders represent surfaces where a greater concentration of donor species is expected from enrichment by Nb defects. Advantages from interfacial junctions can offer improved electrocatalysts, specifically in anode operations with CO present.

Eventually, all active surfaces of the Pt catalyst will get inundated by CO molecules at low temperatures. By selecting an optimum set of conditions to exercise greater productivity over longer intervals that reduces periodic cleansing and lowers stripping potentials, a more resilient anode can be designed. Support buffering effects can also protect carbon from corrosion and limit dissolution. Defect engineering and the interaction between material phases can improve activity and stability in its environment. In all cases, it is important to study catalysts in conditions similar to those found in real scenarios. The hydrogen pump serves as an excellent example for CO tolerance in the anode. Truly, a better set of controls is needed for deeper understanding on the influence of electrochemical potential in metal oxide defects used to form reactive electron–hole pairs. Additional materials characterization of electronic states, especially among metal oxide supports during operation and post-mortem would have been useful in developing this discussion further. Future study could focus on other support compositions with respect to their acceptor and donor relations. Some catalyst properties can be developed beyond geometry, crystal epitaxy, lattice parameters, and strictly metallic considerations by starting with support interactions. These fundamental principles should be used to build electrocatalysts from the bottom up. It was not specifically the goal of this research to establish electronic interactions; rather, an example of a composite metal oxide supported catalyst is integrated into working electrodes to confirm and unify work completed by many others while also contributing insight to principles guiding the design of electrocatalysts for related applications.

4. Conclusions

The design of supports in the electrocatalyst is crucial to their performance and durability. In the anode of polymer electrolyte cells, there is a vital concern from the contamination of hydrogen fuel by carbon monoxide. Bifunctional reactivity of platinum can be improved by the addition of select metal oxides to the surface of multi-wall carbon nanotube supports. Specifically, titania was donor doped with niobium in construction of stable electrocatalysts used in anodes with the best tolerance to 100 ppm carbon monoxide during hydrogen oxidation when compared to a set of controls with and without titania. The anodes were tested in electrochemical hydrogen pumps to characterize their performance and study the synergistic relationship. Resilient behavior in working electrodes can be recognized by forming catalyst junctions with titania and carbon composite supports.

Acknowledgments

This work was completed by the authors at the University of South Carolina in the Horizon I facility. It was supported by the USC – City of Columbia Fuel Cell Collaborative. Dr. Scott Greenway enabled useful interactions and also offered critical review. Assistance of some experiments was provided by Mrs. Diana Larrabee, undergraduate Magellan Scholar. XPS surveys were performed by Dr. Shuguo Ma in our College of Engineering and Computing. TEM and STEM/EDX images were collected by Dr. Haijun Qian at the Clemson University Electron Microscopy Facility.

References

[1] S.J. Lee, S. Mukerjee, E.A. Ticianelli, J. McBreen, Electrochim. Acta 44 (1999) 3283–3293.
[2] H.A. Gasteiger, N.M. Markovic, P.N. Ross Jr., J. Phys. Chem. 99 (1995) 8290–8301.
[3] H.A. Gasteiger, N.M. Markovic, P.N. Ross Jr., J. Phys. Chem. 99 (1995) 16757–16767.
[4] J.E. Hu, J.B. Pearlman, G.S. Jackson, C.J. Tesluk, J. Power Sources 195 (2010) 1926–1935.
[5] S.M.M. Ehteshami, S.H. Chan, Electrochim. Acta 93 (2013) 334–345.
[6] Z. Peng, H. Yang, Nano Today 4 (2009) 143–164.
[7] S.M.M. Ehteshami, Q. Jia, A. Halder, S.H. Chan, S. Mukerjee, Electrochim. Acta 107 (2013) 155–163.
[8] S. Mukerjee, R.C. Urian, Electrochim. Acta 47 (2002) 3219–3231.

[9] F. Micoud, F. Maillard, A. Bonnefont, N. Job, M. Chatenet, Phys. Chem. Chem. Phys. 12 (2010) 1182.
[10] P. Strasser, Q. Fan, M. Devenney, W.H. Weinberg, J. Phys. Chem. B 107 (2003) 11013–11021.
[11] P. Piela, C. Eickes, E. Brosha, F. Garzon, P. Zelenay, J. Electrochem. Soc. 151 (2004) A2053.
[12] G.-S. Park, C. Pak, Y.-S. Chung, J.-R. Kim, W.S. Jeon, Y.-H. Lee, K. Kim, H. Chang, D. Seung, J. Power Sources 176 (2008) 484–489.
[13] J.E. Hu, Z. Liu, B.W. Eichhorn, G.S. Jackson, Int. J. Hydrogen Energy 37 (2012) 11268–11275.
[14] Z. Liu, G.S. Jackson, B.W. Eichhorn, Angew. Chem. Int. Ed. 49 (2010) 3173–3176.
[15] F.J. Scott, S. Mukerjee, D.E. Ramaker, J. Phys. Chem. C 114 (2010) 442–453.
[16] K. Kanda, Z. Noda, Y. Nagamatsu, T. Higashi, S. Taniguchi, S.M. Lyth, A. Hayashi, K. Sasaki, ECS Electrochem. Lett. 3 (2014) F15–F18.
[17] J.J. Pietron, M.B. Pomfret, C.N. Chervin, J.W. Long, D.R. Rolison, J. Mater. Chem. 22 (2012) 5197.
[18] Z. Liu, J.E. Hu, Q. Wang, K. Gaskell, A.I. Frenkel, G.S. Jackson, B. Eichorn, J. Am. Chem. Soc. Commun. 131 (2009) 6924–6925.
[19] H.P. Dhar, L.G. Christner, A.K. Kush, H.C. Maru, J. Electrochem. Soc. 133 (1986) 1574–1582.
[20] S.A. Bilmes, J. Electrochem. Soc. 127 (1980) 2184–2187.
[21] S. Balasubramanian, C.E. Holland, J.W. Weidner, Electrochem. Solid State Lett. 13 (2010) B5.
[22] A. Taniguchi, T. Akita, K. Yasuda, Y. Miyazaki, J. Power Sources 130 (2004) 42–49.
[23] S. Maass, F. Finsterwalder, G. Frank, R. Hartmann, C. Merten, J. Power Sources 176 (2008) 444–451.
[24] Y. Shao-Horn, W.C. Sheng, S. Chen, P.J. Ferreira, E.F. Holby, D. Morgan, Top. Catal. 46 (2007) 285–305.
[25] S. Zhang, X. Yuan, H. Wang, W. Merida, H. Zhu, J. Shen, S. Wu, J. Zhang, Int. J. Hydrogen Energy 34 (2009) 388–404.
[26] M. Oezaslan, F. Hasché, P. Strasser, J. Phys. Chem. Lett. 4 (2013) 3273–3291.
[27] X. Huang, K.L. Reifsnider, in: U. Pasogullari, C.-Y. Chang (Eds.), Mod. Aspects Electrochem., 2010, pp. 1–43.
[28] M. Pourbaix, Atlas of Electrochemical Equilibria in Aqueous Solutions, 1974.
[29] E. Asselin, T.M. Ahmed, A. Alfantazi, Corros. Sci. 49 (2007) 694–710.
[30] T. Mori, D.R. Ou, J. Zou, J. Drennan, Prog. Nat. Sci. Mater. Int. 22 (2012) 561–571.
[31] J. Masud, M.T. Alam, M.R. Miah, T. Okajima, T. Ohsaka, Electrochem. Commun. 13 (2011) 86–89.
[32] Z. Awaludin, M. Suzuki, J. Masud, T. Okajima, T. Ohsaka, J. Phys. Chem. C 115 (2011) 25557–25567.
[33] N.R. de Tacconi, C.R. Chenthamarakshan, K. Rajeshwar, W.-Y. Lin, T.F. Carlson, L. Nikiel, W.A. Wampler, S. Sambandam, V. Ramani, J. Electrochem. Soc. 155 (2008) B1102–B1109.
[34] S. Wendt, R. Schaub, J. Matthiesen, E.K. Vestergaard, E. Wahlström, M.D. Rasmussen, P. Thostrup, L.M. Molina, E. Lægsgaard, I. Stensgaard, B. Hammer, F. Besenbacher, Surf. Sci. 598 (2005) 226–245.
[35] J. Nowotny, T. Bak, M.K. Nowotny, L.R. Sheppard, J. Phys. Chem. B 110 (2006) 18492–18495.
[36] J.M. Jaksic, N.V. Krstajic, L.M. Vracar, S.G. Neophytides, D. Labou, P. Falaras, M.M. Jaksic, Electrochim. Acta 53 (2007) 349–361.
[37] J.M. Jaksic, D. Labou, C.M. Lacnjevac, A. Siokou, M.M. Jaksic, Appl. Catal. A 380 (2010) 1–14.
[38] O. Bikondoa, C.L. Pang, R. Ithnin, C.A. Muryn, H. Onishi, G. Thornton, Nat. Mater. 5 (2006) 189–192.
[39] U. Diebold, Surf. Sci. Rep. 48 (2003) 53–229.
[40] X. Chen, S.S. Mao, Chem. Rev. 107 (2007) 2891–2959.
[41] S.-Y. Huang, P. Ganesan, B.N. Popov, Appl. Catal. B 102 (2011) 71–77.
[42] H. Chhina, D. Susac, S. Campbell, O. Kesler, Electrochem. Solid State Lett. 12 (2009) B97.
[43] A. Bauer, R. Hui, A. Ignaszak, J. Zhang, D.J. Jones, J. Power Sources 210 (2012) 15–20.
[44] K.Y. Chen, Electrochem. Solid State Lett. 3 (1999) 10.
[45] D.-J. Guo, X.-P. Qiu, L.-Q. Chen, W.-T. Zhu, Carbon 47 (2009) 1680–1685.
[46] B.Y. Xia, B. Wang, H.B. Wu, Z. Liu, X. Wang, X.W. Lou, J. Mater. Chem. 22 (2012) 16499–16505.
[47] C. Ma, Y. Jin, M. Shi, Y. Chu, Y. Xu, W. Jia, Q. Yuan, J. Chen, D. Chen, S. Chen, J. Electrochem. Soc. 161 (2013) F246–F251.
[48] G. Sakai, T. Arai, T. Matsumoto, T. Ogawa, M. Yamada, K. Sekizawa, T. Taniguchi, ChemElectroChem 1 (2014) 366–370.
[49] J. Zhu, X. Zhao, M. Xiao, L. Liang, C. Liu, J. Liao, W. Xing, Carbon 72 (2014) 114–124.
[50] R. Kou, Y. Shao, D. Mei, Z. Nie, D. Wang, C. Wang, V.V. Viswanathan, S. Park, I.A. Aksay, Y. Lin, Y. Wang, J. Liu, J. Am. Chem. Soc. 133 (2011) 2541–2547.
[51] N.G. Akalework, C.-J. Pan, W.-N. Su, J. Rick, M.-C. Tsai, J.-F. Lee, J.-M. Lin, L.-D. Tsai, B.-J. Hwang, J. Mater. Chem. 22 (2012) 20977–20985.
[52] N. Zhang, S. Zhang, C. Du, Z. Wang, Y. Shao, F. Kong, Y. Lin, G. Yin, Electrochim. Acta 117 (2014) 413–419.
[53] J. Wang, J. Xi, Y. Bai, Y. Shen, J. Sun, L. Chen, W. Zhu, X. Qiu, J. Power Sources 164 (2007) 555–560.
[54] D.-M. Gu, Y.-Y. Chu, Z.-B. Wang, Z.-Z. Jiang, G.-P. Yin, Y. Liu, Appl. Catal. B 102 (2011) 9–18.
[55] B. Ruiz Camacho, C. Morais, M.A. Valenzuela, N. Alonso-Vante, Catal. Today 202 (2013) 36–43.
[56] K. Huang, K. Sasaki, R.R. Adzic, Y. Xing, J. Mater. Chem. 22 (2012) 16824.
[57] P. Trogadas, V. Ramani, J. Electrochem. Soc. 155 (2008) B696–B703.
[58] J. Nowotny, T. Bak, M.K. Nowotny, L.R. Sheppard, J. Phys. Chem. C 112 (2008) 590–601.
[59] J. Nowotny, T. Bak, M.K. Nowotny, L.R. Sheppard, J. Phys. Chem. C 112 (2008) 602–610.
[60] D.M. Smyth, The Defect Chemistry of Metal Oxides, 2000.
[61] L.R. Sheppard, T. Bak, J. Nowotny, J. Phys. Chem. B 110 (2006) 22447–22454.
[62] K. Sasaki, J. Maier, J. Appl. Phys. 86 (1999) 5422–5433.
[63] K. Sasaki, J. Maier, J. Appl. Phys. 86 (1999) 5434–5443.
[64] L.R. Sheppard, T. Bak, J. Nowotny, J. Phys. Chem. B 110 (2006) 22455–22461.
[65] D.D. Mulmi, T. Sekiya, N. Kamiya, S. Kurita, Y. Murakami, T. Kodaira, J. Phys. Chem. Solids 65 (2004) 1181–1185.
[66] E. Comini, M. Ferroni, V. Guidi, A. Vomiero, P.G. Merli, V. Morandi, M. Sacerdoti, G.D. Mea, G. Sberveglieri, Sensors Actuators B Chem. 108 (2005) 21–28.
[67] J. Robertson, Phys. Status Solidi A 207 (2010) 261–269.
[68] W.M. Haynes (Ed.), CRC Handbook of Chemistry and Physics, 2013–2014.
[69] Y. Liu, J.M. Szeifert, J.M. Feckl, B. Mandlmeier, J. Rathousky, O. Hayden, D. Fattakhova-Rohlfing, T. Bein, ACS Nano 4 (2010) 5373–5381.
[70] J. Tao, H. Pan, L.M. Wong, T.I. Wong, J.W. Chai, J. Pan, S.J. Wang, Mater. Res. Express 1 (2014) 015911.
[71] M.K. Nowotny, L.R. Sheppard, T. Bak, J. Nowotny, J. Phys. Chem. C 112 (2008) 5275–5300.
[72] D. Morris, Y. Dou, J. Rebane, C.E.J. Mitchell, R.G. Egdell, D.S.L. Law, A. Vittadini, M. Casarin, Phys. Rev. B 61 (2000) 13445–13457.
[73] D. Wang, C.V. Subban, H. Wang, E. Rus, F.J. DiSalvo, H.D. Abruña, J. Am. Chem. Soc. Commun. 132 (2010) 10218–10220.
[74] A. Kumar, V. Ramani, ACS Catal. 4 (2014) 1516–1525.
[75] A. Kumar, V. Ramani, J. Electrochem. Soc. 160 (2013) F1207–F1215.
[76] M.M. Jaksic, G.A. Botton, G.D. Papakonstantinou, F. Nan, J.M. Jaksic, J. Phys. Chem. C 118 (2014) 8723–8746.
[77] X. Liu, X. Wu, K. Scott, Catalysis Science & Technology, 2014.
[78] S.J. Tauster, S.C. Fung, R.T.K. Baker, J.A. Horsley, Science 211 (1981) 1121–1125.
[79] S.J. Tauster, S.C. Fung, R.L. Garten, J. Am. Chem. Soc. 100 (1978) 170–175.
[80] O. Dulub, W. Hebenstreit, U. Diebold, Phys. Rev. Lett. 84 (2000) 3646–3649.
[81] S. Bonanni, K. Aït-Mansour, H. Brune, W. Harbich, ACS Catal. 1 (2011) 385–389.
[82] Y. Zhou, C.L. Muhich, B.T. Neltner, A.W. Weimer, C.B. Musgrave, J. Phys. Chem. C 116 (2012) 12114–12123.
[83] S.G. Neophytides, S.H. Zafeiratos, M.M. Jaksic, J. Electrochem. Soc. 150 (2003) E512.
[84] J.M. Jaksic, D. Labou, G.D. Papakonstantinou, A. Siokou, M.M. Jaksic, J. Phys. Chem. C 114 (2010) 18298–18312.
[85] L.R. Baker, A. Hervier, H. Seo, G. Kennedy, K. Komvopoulos, G.A. Somorjai, J. Phys. Chem. C 115 (2011) 16006–16011.
[86] D.-e. Jiang, S.H. Overbury, S. Dai, J. Phys. Chem. C 116 (2012) 21880–21885.
[87] S.C. Ammal, A. Heyden, J. Phys. Chem. C 115 (2011) 19246–19259.
[88] C.L. Muhich, Y. Zhou, A.M. Holder, A.W. Weimer, C.B. Musgrave, J. Phys. Chem. C 116 (2012) 10138–10149.
[89] Z. Jiang, Y. Yang, W. Shangguan, Z. Jiang, J. Phys. Chem. C 116 (2012) 19396–19404.
[90] G.A. Hope, A.J. Bard, J. Phys. Chem. 87 (1983) 1979–1984.
[91] J.Y. Park, J.R. Renzas, A.M. Contreras, G.A. Somorjai, Top. Catal. 46 (2007) 217–222.
[92] R.E. Fuentes, B.L. Garcia, J.W. Weidner, J. Electrochem. Soc. 158 (2011) B461.
[93] G. Chen, S.R. Bare, T.E. Mallouk, J. Electrochem. Soc. 149 (2002) A1092–A1099.
[94] C.-S. Chen, F.-M. Pan, Appl. Catal. B 91 (2009) 663–669.
[95] X. Zhao, J. Zhu, L. Liang, J. Liao, C. Liu, W. Xing, J. Mater. Chem. 22 (2012) 19718.
[96] F. Shi, L.R. Baker, A. Hervier, G.A. Somorjai, K. Komvopoulos, Nano Lett. 13 (2013) 4469–4474.
[97] P. Stonehart, D. Wheeler, Mod. Asp. Electrochem. 38 (2005) 373–424.
[98] J.R.C. Salgado, R.G. Duarte, L.M. Ilharco, A.M. Botelho do Rego, A.M. Ferraria, M.G.S. Ferreira, Appl. Catal. B 102 (2011) 496–504.
[99] R. Escudero-Cid, A.S. Varela, P. Hernández-Fernández, E. Fatás, P. Ocón, Int. J. Hydrogen Energy 39 (2014) 5063–5073.
[100] F. Hasché, M. Oezaslan, P. Strasser, Phys. Chem. Chem. Phys. 12 (2010) 15251.
[101] Y. Shao, G. Yin, Y. Gao, P. Shi, J. Electrochem. Soc. 153 (2006) A1093.
[102] Z. Tang, H.Y. Ng, J. Lin, A.T.S. Wee, D.H.C. Chua, J. Electrochem. Soc. 157 (2010) B245.
[103] M.S. Saha, A. Kundu, J. Power Sources 195 (2010) 6255–6261.
[104] A.O. Al-Youbi, J.L. Gómez de la Fuente, F.J. Pérez-Alonso, A.Y. Obaid, J.L.G. Fierro, M.A. Peña, M. Abdel Salam, S. Rojas, Appl. Catal. B 150–151 (2014) 21–29.
[105] A.K. Roy, C.-T. Hsieh, Electrochim. Acta 87 (2013) 63–72.
[106] N.-Y. Hsu, C.-C. Chien, K.-T. Jeng, Appl. Catal. B 84 (2008) 196–203.
[107] A. Guha, W. Lu, T.A. Zawodzinski, D.A. Schiraldi, Carbon 45 (2007) 1506–1517.
[108] X. Li, H. Wang, H. Yu, Z. Liu, F. Peng, J. Power Sources 260 (2014) 1–5.

[109] K. Jukk, J. Kozlova, P. Ritslaid, V. Sammelselg, N. Alexeyeva, K. Tammeveski, J. Electroanal. Chem. 708 (2013) 31–38.
[110] F. Alcaide, G. Álvarez, O. Miguel, M.J. Lázaro, R. Moliner, A. López-Cudero, J. Solla-Gullón, E. Herrero, A. Aldaz, Electrochem. Commun. 11 (2009) 1081–1084.
[111] S. Sharma, A. Ganguly, P. Papakonstantinou, X. Miao, M. Li, J.L. Hutchinson, M. Delichatsios, S. Ukleja, J. Phys. Chem. C 114 (2010) 19459–19466.
[112] X. Li, W.-X. Chen, J. Zhao, W. Xing, Z.-D. Xu, Carbon 43 (2005) 2168–2174.
[113] A. Jitianu, T. Cacciaguerra, M.-H. Berger, R. Benoit, F. Béguin, S. Bonnamy, J. Non Cryst. Solids 345–346 (2004) 596–600.
[114] A.J. Atanacio, T. Bak, J. Nowotny, J. Phys. Chem. C 118 (2014) 11174–11185.
[115] Z.Q. Tian, S.P. Jiang, Y.M. Liang, P.K. Shen, J. Phys. Chem. B 110 (2006) 5343–5350.
[116] X. Huang, W. Rigdon, J. Neutzler, D. Larrabee, J. Sightler, ECS Trans. 41 (2011) 901–907.
[117] W.A. Rigdon, X. Huang, T.I. Valdez, ECS Meet. Abstr. 224 (2013), 1507–1507.
[118] M. Chisaka, A. Ishihara, K.-i. Ota, H. Muramoto, Electrochim. Acta 113 (2013) 735–740.
[119] A. Jitianu, T. Cacciaguerra, R. Benoit, S. Delpeux, F. Béguin, S. Bonnamy, Carbon 42 (2004) 1147–1151.
[120] Z.-Z. Jiang, Z.-B. Wang, Y.-Y. Chu, D.-M. Gu, G.-P. Yin, Energy Environ. Sci. 4 (2011) 2558.
[121] J. Shim, C.-R. Lee, H.-K. Lee, J.-S. Lee, E.J. Cairns, J. Power Sources 102 (2001) 172–177.
[122] W.F. Zhang, Y.L. He, M.S. Zhang, Y. Zin, Q. Chen, J. Appl. Phys. D 33 (2000) 912–916.
[123] W.F. Zhang, M.S. Zhang, Z. Yin, Q. Chen, Appl. Phys. B 70 (2000) 261–265.
[124] A. Naldoni, M. Allieta, S. Santangelo, M. Marelli, F. Fabbri, S. Cappelli, C.L. Bianchi, R. Psaro, V. Dal Santo, J. Am. Chem. Soc. 134 (2012) 7600–7603.
[125] S.X. Zhang, D.C. Kundaliya, W. Yu, S. Dhar, S.Y. Young, L.G. Salamanca-Riba, S.B. Ogale, R.D. Vispute, T. Venkatesan, J. Appl. Phys. 102 (2007) 013701.
[126] A.M. Ruiz, G. Dezanneau, J. Arbiol, A. Cornet, J.R. Morante, Chem. Mater. 16 (2004) 862–871.
[127] S. Osswald, M. Havel, Y. Gogotsi, J. Raman Spectrosc. 38 (2007) 728–736.
[128] Z. Awaludin, J.G. Sheng Moo, T. Okajima, T. Ohsaka, J. Mater. Chem. A 1 (2013) 14754–14765.
[129] X. Guo, D.-J. Guo, X.-P. Qiu, L.-Q. Chen, W.-T. Zhu, J. Power Sources 194 (2009) 281–285.
[130] L. Timperman, Y.J. Feng, W. Vogel, N. Alonso-Vante, Electrochim. Acta 55 (2010) 7558–7563.
[131] U. Diebold, J.-M. Pan, T. Madey, Surf. Sci. 331–333 (1995) 845–854.
[132] J.A. Horsley, J. Am. Chem. Soc. 101 (1978) 2870–2874.
[133] S.A. Chambers, Y. Gao, Y.J. Kim, M.A. Henderson, S. Thevuthasan, S. Wen, K.L. Merkle, Surf. Sci. 365 (1996) 625–637.
[134] A. Lewera, L. Timperman, A. Roguska, N. Alonso-Vante, J. Phys. Chem. C 115 (2011) 20153–20159.
[135] J.-H. Kim, S. Chang, Y.-T. Kim, Appl. Catal. B 158-159 (2014) 112–118.
[136] X. Wang, J.C. Yu, H.Y. Yip, L. Wu, P.K. Wong, S.Y. Lai, Chem. A Eur. J. 11 (2005) 2997–3004.
[137] L. Yan, K. Huang, Y. Chen, Y. Xing, ECS Electrochem. Lett. 3 (2014) F27–F29.
[138] D.R. Ou, T. Mori, K. Fugane, H. Togasaki, F. Ye, J. Drennan, J. Phys. Chem. C 115 (2011) 19239–19245.
[139] L. Zhang, L. Wang, C.M.B. Holt, B. Zahiri, Z. Li, K. Malek, T. Navessin, M.H. Eikerling, D. Mitlin, Energy Environ. Sci. 5 (2012) 6156.
[140] K. Huang, Y. Li, L. Yan, Y. Xing, RSC Adv. 4 (2014) 9701–9708.
[141] C. Xu, P. Pietrasz, J. Yang, R. Soltis, K. Sun, M. Sulek, R. Novak, ECS Trans. 58 (2013) 1779–1788.
[142] B.B. Blizanac, S. Pylypenko, T.S. Olson, D. Konopka, P. Atanassov, J. Electrochem. Soc. 158 (2011) B485.
[143] D.A. Konopka, M. Li, K. Artyushkova, N. Marinkovic, K. Sasaki, R. Adzic, T.L. Ward, P. Atanassov, J. Phys. Chem. C 115 (2011) 3043–3056.
[144] D. Konopka, B. Kiefer, Y.-B. Jiang, T. Ward, P. Atanassov, J. Electrochem. Soc. 158 (2011) B804.
[145] Y. Fan, Z. Yang, P. Huang, X. Zhang, Y.-M. Liu, Electrochim. Acta 105 (2013) 157–161.
[146] B. Ruiz-Camacho, H.H.R. Santoyo, J.M. Medina-Flores, O. Álvarez-Martínez, Electrochim. Acta 120 (2014) 344–349.
[147] K.R. Cooper, V. Ramani, J.M. Fenton, H.R. Kunz, Experimental Methods and Data Analyses for Polymer Electrolyte Fuel Cells, Scribner Associates, Inc., Southern Pines, NC, 2005.
[148] K. Kinoshita, P. Stonehart, in: J.O.M. Bockris, B.E. Conway (Eds.), Mod. Aspects Electrochem., Springer, US, 1977, pp. 183–266.
[149] W.A. Rigdon, D. Larrabee, X. Huang, ECS Trans. 58 (2013) 1809–1821.
[150] Z. Xu, H. Zhang, H. Zhong, Q. Lu, Y. Wang, D. Su, Appl. Catal. B 111–112 (2012) 264–270.
[151] G. Chen, Y. Tan, B. Wu, G. Fu, N. Zheng, Chem. Commun. 48 (2012) 2758.
[152] N. Tian, Z.Y. Zhou, S.G. Sun, Y. Ding, Z.L. Wang, Science 316 (2007) 732–735.
[153] R. Imbihl, G. Ertl, Chem. Rev. 95 (1995) 697–733.
[154] N. Wagner, E. Gülzow, J. Power Sources 127 (2004) 341–347.
[155] Y. Gao, Y. Liang, S.A. Chambers, Surf. Sci. 365 (1996) 638–648.